DOI: 10.1002/chem.200902161

VIP

Dendritic Porphyrin–Fullerene Conjugates: Efficient Light-Harvesting and Charge-Transfer Events

Sebastian Schlundt,[a] Gregory Kuzmanich,[b] Fabian Spänig,[c] Gustavo de Miguel Rojas,[c] Christian Kovacs,[a] Miguel A. Garcia-Garibay,*[b] Dirk. M. Guldi,*[c] and Andreas Hirsch*[a]

Abstract: A novel dendritic C_{60}-H_2P-$(ZnP)_3$ (P = porphyrin) conjugate gives rise to the successful mimicry of the primary events in photosynthesis, that is, light harvesting, unidirectional energy transfer, charge transfer, and charge-shift reactions. Owing, however, to the flexibility of the linkers that connect the C_{60}, H_2P, and ZnP units, the outcome depends strongly on the rigidity/viscosity of the environment. In an agar matrix or Triton X-100, time-resolved transient absorption spectroscopic analysis and fluorescence-lifetime measurements confirm the following sequence. Initially, light harvesting is seen by the peripheral C_{60}-H_2P-*$(ZnP)_3$ conjugate. Once photoexcited, a unidirectional energy transfer funnels the singlet excited-state energy to H_2P to form C_{60}-*(H_2P)-$(ZnP)_3$, which powers an intramolecular charge transfer that oxidizes the photoexcited H_2P and reduces the adjacent C_{60} species. In the correspondingly formed $(C_{60})^{\bullet-}$-$(H_2P)^{\bullet+}$-$(ZnP)_3$ conjugate, an intramolecular charge-shift reaction generates $(C_{60})^{\bullet-}$-H_2P-$(ZnP)_3^{\bullet+}$, in which the radical cation resides on one of the three ZnP moieties, and for which lifetimes of up to 460 ns are found. On the other hand, investigations in organic media (i.e., toluene, THF, and benzonitrile) reveal a short cut, that is, the peripheral ZnP unit reacts directly with C_{60} to form $(C_{60})^{\bullet-}$-H_2P-$(ZnP)_3^{\bullet+}$. Substantial configurational rearrangements—placing ZnP and C_{60} in proximity to each other—are, however, necessary to ensure the required through space interactions (i.e., close approach). Consequently, the lifetime of $(C_{60})^{\bullet-}$-H_2P-$(ZnP)_3^{\bullet+}$ is as short as 100 ps in benzonitrile.

Keywords: dendrimers · electron transfer · fullerenes · photochemistry · porphyrinoids

Introduction

Light conversion in plants and photosynthetic bacteria is one of the fundamental processes that governs life on earth. In fact, energy in the form of sunlight is harvested to power the processes of life and to build up organic material. The bacterial photosynthetic reaction center provides meaningful incentives for the optimization of charge-separation processes in artificial model systems.[1,2] Common to all these systems is a relay of short-range energy/electron-transfer reactions that evolve among chlorophyll and quinone moieties. Importantly, the primary electron-transfer processes of photosynthesis are characterized by an extremely small reorganization energy (0.2 eV) attained by the transmembrane protein environment. Owing to the importance and complexity of natural photosynthesis, the study thereof necessitates suitable simpler models. The ultimate goal is to design and assemble synthetic systems that can efficiently convert solar energy into useful chemical energy.[3–6] Porphyrinoids, especially metalloporphyrinoid systems with their rich and exten-

[a] S. Schlundt, C. Kovacs, Prof. Dr. A. Hirsch
Department of Chemistry and Pharmacy and
Interdisciplinary Center of Molecular Materials (ICMM)
Friedrich-Alexander-Universität Erlangen-Nürnberg
Henkestrasse 42, 91054-Erlangen (Germany)
Fax: (+49) 9131-852-6864
E-mail: andreas.hirsch@chemie.uni-erlangen.de

[b] G. Kuzmanich, Prof. Dr. M. A. Garcia-Garibay
Department of Chemistry and Biochemistry
University of California
Los Angeles, CA 90024-1569 (USA)
Fax: (+1) 310-825-0767
E-mail: mgg@chem.ucla.edu

[c] F. Spänig, Dr. G. de Miguel Rojas, Prof. Dr. D. M. Guldi
Department of Chemistry and Pharmacy and
Interdisciplinary Center of Molecular Materials (ICMM)
Friedrich-Alexander-Universität Erlangen-Nürnberg
Egerlandstrasse 3, 91058-Erlangen (Germany)
Fax: (+49) 9131-852-7340
E-mail: dirk.guldi@chemie.uni-erlangen.de

Supporting information for this article is available on the WWW under http://dx.doi.org/10.1002/chem.200902161.

sive absorptions throughout the visible region of the solar spectrum, hold particularly great promise as integrative building blocks with increased absorptive cross sections. This finding led to the establishment of synthetic methodologies that allowed porphyrins and metalloporphyrins—as excited-state electron donors—to be linked to electron acceptors, such as fullerenes.[7–16] Since the initial discovery of fullerenes, chemists and physicists worldwide have studied their solid-state properties, ranging from superconductivity and nanostructured devices to endohedral fullerene chemistry. The three-dimensional, spherical structure of fullerenes, which are made of alternating hexagons (i.e., electron rich) and pentagons (i.e., electron deficient) with diameters starting at 7.8 Å for C_{60}, evoked a lively interest in relating their properties to conventional two-dimensional π systems. Their extraordinary electron-acceptor properties—predicted theoretically and confirmed experimentally—have resulted in noteworthy advances in the areas of light-induced electron-transfer chemistry and solar-energy conversion.[17,18] It is mainly the small reorganization energy that fullerenes exhibit in electron-transfer reactions which is accountable for this breakthrough. In particular, ultrafast charge-separation and very slow charge-recombination features lead to unprecedented long-lived radical ion pair states formed with high quantum efficiencies.[19] Only, through the design and development of light harvesting, photoconversion, and catalytic modules capable of self-ordering and self-assembling into an integrated functional unit will it be possible to realize efficient artificial photosynthetic systems. Should charges, however, be transported over distances larger than 20 Å alternative concepts have to be applied. This task becomes particularly relevant when achieving ultralong radical-ion-pair lifetimes. A viable option to achieve long-distance, charge-separated states makes use of a relay of several short-range electron-transfer steps along well-designed redox gradients rather than forcing the electron transfer through a single, concerted long-range step. Such a "relay concept" has been successfully realized by combining several redox active building blocks. Herein, we focused on ZnP, H_2P, and C_{60} species (P = porphyrin). This approach is expected to lead to a scenario in which the final electron donors (i.e., ZnP) and the primary electron acceptors (i.e., C_{60}) form a spatially separated radical ion pair $(C_{60})^{\bullet-}$-H_2P-$(ZnP)_3^{\bullet+}$.

Light harvesting is another topic that needs to be addressed in designing artificial photosynthetic systems that will ultimately power the practical production of solar fuels.[20] Three light-harvesting complexes LH1, LH2, and LH3 are found in bacteria. These complexes consist of porphyrin arrays that are embedded in a protein matrix that can harvest light over a broad range of the solar spectrum and funnel its excited-state energy to the reaction center. Artificial light harvesting can be achieved by means of dendritic architectures attached to C_{60}, which renders these systems particularly appealing for photoconversion processes. Placing four chromophores, that is, three ZnP and one H_2P units, in C_{60}-H_2P-$(ZnP)_3$ at the fullerene periphery enhances, for example, the light-collection and light-transduction features of the resulting core-shell ensembles. Ultimately, this approach may lead to high solar-energy conversion efficiencies. In fact, we demonstrate that C_{60}-H_2P-$(ZnP)_3$ shows the two basic functions of photosynthesis, namely, light harvesting and charge transfer.

Results and Discussion

Synthesis: Porphyrin **5**[21] (Scheme 1) was synthesized by a statistical condensation of aldehyde **3**[22] (3 equiv), aldehyde **4**[23] (1 equiv), and pyrrole (4 equiv) under conditions developed by Lindsey and co-workers[24] in CH_2Cl_2. Boron trifluoride etherate was used as a Lewis acid catalyst, ethanol and PPh_4Cl as co-catalysts, and 2,3-dichloro-5,6-dicyano-1,4-benzoquinone (DDQ) as an oxidizing agent. The product was purified by column chromatography. Cyclopropanation of C_{60} was achieved with a modification of the conditions developed by Bingel.[25] Porphyrin **5**,[21] C_{60}, and iodine were dissolved in toluene, and diluted 1,8-diazabicyclo-[5.4.0]undec-7-ene (DBU) was added slowly. After two days of stirring, compound **6**[21] was purified by column chromatography (silica, toluene/EtOAc 9:1) and precipitated in

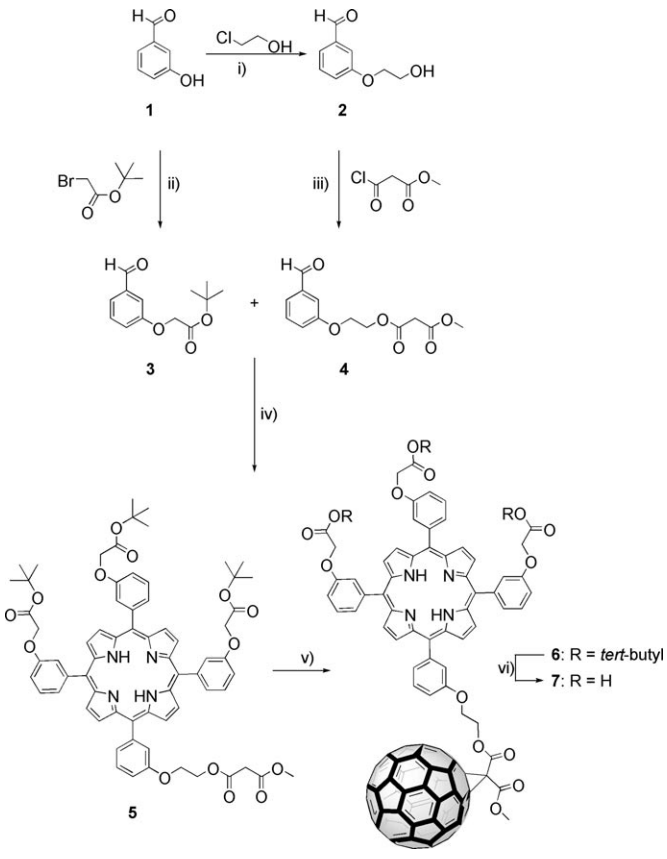

Scheme 1. Synthesis of porphyrin **5**[21] and dyad **7**. i) NaOH, H_2O, reflux (68%); ii) NaOH, H_2O, CH_2Cl_2, tetrabutylammonium bromide; iii) pyridine, CH_2Cl_2, 0 °C; iv) pyrrole, boron trifluoride etherate, PPh_4Cl, ethanol, DDQ, CH_2Cl_2; v) iodine, DBU, C_{60}, toluene; vi) formic acid. DDQ = 2,3-dichloro-5,6-dicyano-1,4-benzoquinone, DBU = 1,8-diazabicyclo-[5.4.0]undec-7-ene.

pentane. Subsequently, the *tert*-butyl protecting groups could be quantitatively removed in formic acid to afford **7**, which was characterized by ^{1}H NMR, ^{13}C NMR, and UV/Vis spectroscopy and MALDI-TOF mass-spectrometric analysis. Compound **7** is one of the major building blocks for the synthesis of dendritic porphyrin–fullerene hybrid **11**.

Porphyrin **9**[26] was also synthesized statistically (by using pyrrole, boron trifluoride etherate, PPh_4Cl, ethanol, DDQ, and CH_2Cl_2) under the conditions developed by Lindsey and co-workers.[24] Subsequently, **10**[26] was obtained from its free-base precursor **9**[26] with fivefold excess of Zn-$(OAc)_2{\cdot}2H_2O$ heated to reflux in THF for 3 hours (Scheme 2).

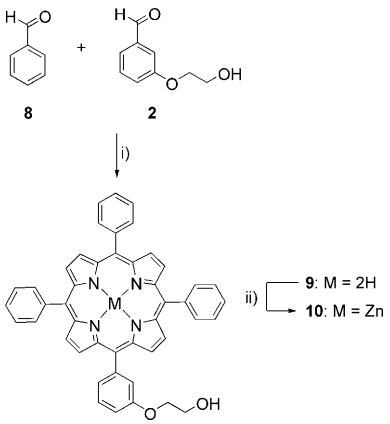

Scheme 2. Synthesis of porphyrin **10**.[26] i) Pyrrole, boron trifluoride etherate, PPh_4Cl, ethanol, DDQ, CH_2Cl_2; ii) $Zn(OAc)_2{\cdot}2H_2O$, THF, reflux.

The two building blocks **7** and **10**[26] were coupled in THF using N,N′-dicyclohexylcarbodiimide (DCC) as the coupling agent (Scheme 3). DCC and porphyrin **10**[26] were added subsequently to a solution of 7,4-dimethylaminopyridine (DMAP) and 1-hydroxybenzotriazole hydrate (HOBT) dissolved in THF at 0 °C. After stirring at room temperature for six days in the dark, additional DCC was added at 0 °C. Precipitated dicyclohexylurea (DCU) was removed after another day of stirring at room temperature. The product was purified by column chromatography (silica gel, CH_2Cl_2/EtOAc 20:0.75, 1 % NEt_3) and recrystallization (CH_2Cl_2/pentane). The porphyrin–fullerene hybrid **11** was characterized by ^{1}H NMR, ^{13}C NMR, UV/Vis, and IR spectroscopy, and MALDI-TOF and ESI mass spectrometry. Because the NMR spectra were recorded in $CDCl_3$ at room temperature, signals were seen that were split into multiplets. For example, the three carbonyl groups of the linking esters gave rise to a series of nine peaks in the ^{13}C NMR spectrum between $\delta = 168.63$ and 168.00 ppm. A feasible rationale implies the presence of different conformers based on π–π stacking of C_{60}/ZnP. Independent confirmation of this assumption came from ^{1}H and ^{13}C NMR spectra at 100 °C in [D_2]tetrachloroethane. At this temperature, the structures formed through π–π interactions are likely to be broken up. In line with such structural arrangements, the three linker carbonyl groups are identified by only one set of signals with two peaks at $\delta = 168.82$ and 168.78 ppm. Similar changes were observed for all the other carbon atoms of **11**.

For comparison, the dendritic structure H_2P-$(ZnP)_3$ **12** was synthesized analogously. Therefore, porphyrin **13** was

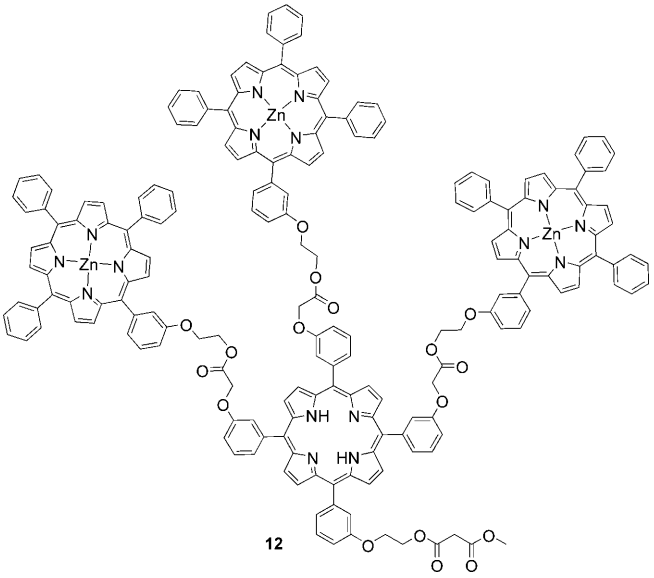

obtained from **5**[21] by treatment with formic acid (Scheme 4). An additional reference fullerene derivative **14**[27] was synthesized according to known protocols for the following photophysical investigations.

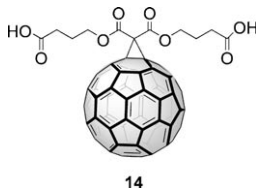

Steady-state absorption spectroscopy: To shed light on the electronic interactions between the photo- and redox-active components (i.e., ZnP, H_2P, and C_{60}), the ground-state absorption spectra of the donor–acceptor ensembles were compared in THF with those of the individual components. At first glance, the absorption spectra of the ensembles might be best described as simple superimpositions of the component spectra that lack notable perturbations or additional charge-transfer transitions. In particular, the dominating Soret and Q bands of the porphyrins are seen in the regions $\lambda = 400$–450 and 550–650 nm, respectively. The strongest bands of the C_{60} units, on the other hand, are at $\lambda = 220$, 265, and 330 nm and extend all the way to the energetically lowest lying transition at $\lambda = 690$ nm. Nevertheless, a closer look reveals subtle changes; for example, the porphyrin Soret and Q bands in **6** are bathochromically shifted by about $\Delta\lambda = 6$ nm relative to **5**. Moreover, **11** gives rise to only one intense Soret band at $\lambda = 425$ nm.

Electrochemistry: The electrochemical properties of all the investigated compounds were studied by cyclic voltammetry and differential pulse voltammetry (DPV) in dichlorome-

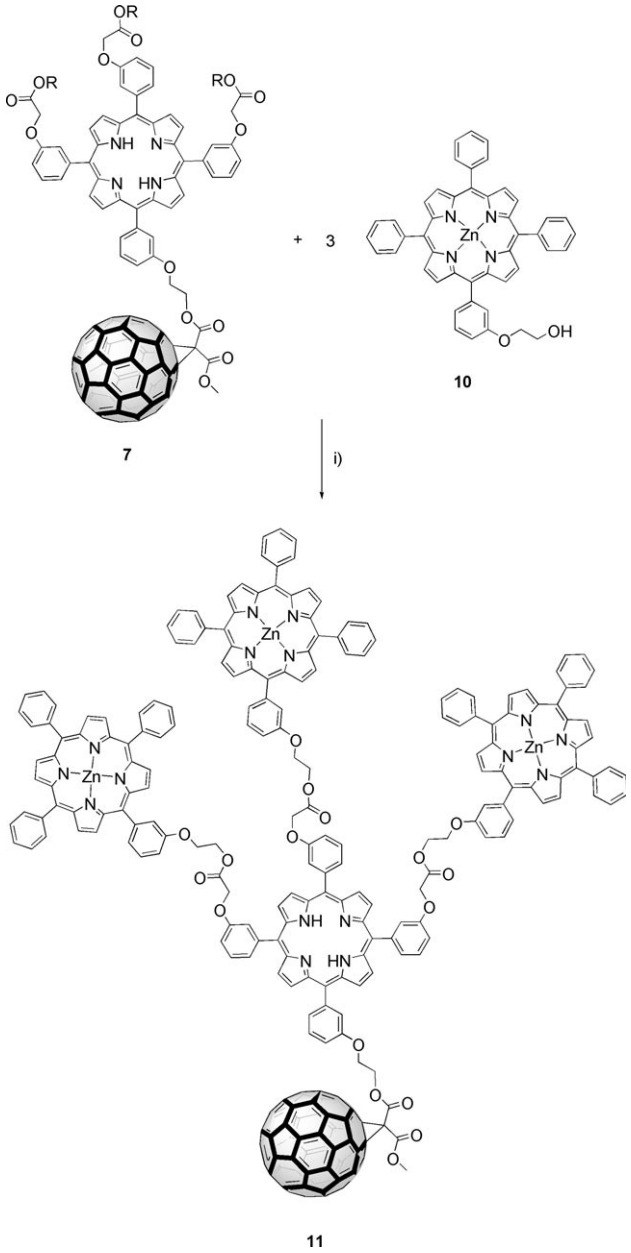

Scheme 3. Synthesis of dendritic porphyrin–fullerene hybrid **11**. i) DMAP, HOBT, DCC, THF. DCC = *N*,*N*′-dicyclohexylcarbodiimide, DMAP = **7**,4-dimethylaminopyridine, HOBT = 1-hydroxybenzotriazole hydrate.

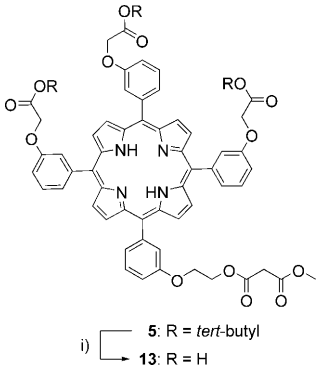

Scheme 4. Porphyrin building block **13**. i) Formic acid, overnight.

thane (Table 1). For **5**, the first and second reversible reductions are seen at −1.66 and −1.96 V, respectively. Reversible oxidation, on the other hand, occurs at +0.58 and +0.91 V. Both the reduction and oxidation are affected in **10** with values of −1.91 and +0.35/+0.75 V, respectively.

In **12**, the reversible reduction of H_2P is shifted to −1.74 V, while that of ZnP is virtually identical to the reference. Overall, the 3:1 ratio is discernable when comparing the areas of the integrated peaks. On the oxidative side, processes at +0.35, +0.60, +0.68, and +1.00 V correspond to the first oxidation of ZnP, the first oxidation of H_2P, the second oxidation of ZnP, and the second oxidation of H_2P, respectively.

Turning to the oxidation of **6**, only H_2P-centered processes emerge at +0.55 and +1.05 V. This behavior infers only slight changes relative to the H_2P reference. In stark contrast, the reduction of **6** involves C_{60}-centered processes at −1.12, −1.47, and −2.04 V as well as H_2P-centered processes at −1.67 and −2.04 V.

With this information in hand, the redox features of **11** evolve as the sum of the C_{60}, H_2P, and ZnP redox properties. Again, oxidation is limited to H_2P and ZnP with values at +0.53/+1.02 and +0.30/+0.65 V, respectively. For the reduction, the following values were derived: −1.17, −1.50, and −2.06 V (C_{60}); −1.70 V (H_2P); −1.91 V (ZnP).

Steady-state fluorescence spectroscopy: The fluorescence spectra of all the reference compounds and all the donor–acceptor conjugates were recorded in solvents of different

Table 1. Electrochemical features of the different donor–acceptor conjugates and the corresponding reference systems recorded in dichloromethane versus ferrocene/ferrocenium.

	$H_2P^{\bullet+}/H_2P^{2+}$	$H_2P/H_2P^{\bullet+}$	$ZnP^{\bullet+}/ZnP^{2+}$	$ZnP/ZnP^{\bullet+}$	$C_{60}/C_{60}^{\bullet-}$	$C_{60}^{\bullet-}/C_{60}^{2-}$	$C_{60}^{2-}/C_{60}^{\bullet 3-}$	$H_2P/H_2P^{\bullet-}$	$ZnP/ZnP^{\bullet-}$
5	0.91	0.58						−1.66	
10			0.75	0.35					−1.91
12	1.00	0.60	0.68	0.35[a]				−1.74	−1.91
14					−1.13	−1.48	−2.03		
6	1.05	0.55			−1.12	−1.47	−2.04	−1.67	
11	1.02	0.53	0.65[a]	0.30	−1.17	−1.50	−2.06	−1.70	−1.91[a]

[a] Taken from DPV.

polarity—toluene, THF, and benzonitrile—and in the absence of molecular oxygen (Table 2). All porphyrins containing conjugates were excited at $\lambda = 420$ nm. Moreover, selective excitation of ZnP was achieved at $\lambda = 560$ nm, whereas H_2P was excited at $\lambda = 647$ nm.

Table 2. Fluorescence features of the different donor–acceptor conjugates and the corresponding reference systems recorded in solvents of different polarity.

		Toluene		THF		Benzonitrile	
	E_{0-0} [eV]	λ_{em} [nm]	Φ_{em} [$\times 10^{-2}$]	τ_{em} [ns]	Φ_{em} [$\times 10^{-2}$]	τ_{em} [ns]	Φ_{em} [$\times 10^{-2}$]	τ_{em} [ns]
5	1.89	649, 715	11.0	9.8	11.0	9.8	11.0	9.8
10	2.04	600, 652	4.0	2.4	4.0	2.4	4.0	2.4
12	2.04	600, 652	0.30[a]	0.21	0.21[a]	0.22	0.29[a]	0.22
	1.89	649, 715	5.95[a]	5.40	6.11[a]	5.76	6.63[a]	5.97
14	1.79	720	0.06	1.8	0.06	1.8	0.06	1.8
6	1.89	649, 715	0.22	0.200[b]	0.20	0.181[b]	0.17	0.154[b]
11	2.04	600, 652	0.08[a]	0.048[b]	0.06[a]	0.036[b]	0.05[a]	0.030[b]
	1.89	649, 715	0.09[a]	0.054[b]	0.09[a]	0.054[b]	0.09[a]	0.054[b]

[a] Determined based on the emission bands at $\lambda = 600$ and 715 nm for ZnP and H_2P, respectively. [b] Estimated from the fluorescence quenching.

Porphyrin derivative **5** exhibits the well-known emission features of analogous compounds of its class, with fluorescence maxima at $\lambda = 659$ and 715 nm, a fluorescence quantum yield Φ of 0.11, and a fluorescence lifetime τ of 9.8 ns.[28–30] Similarly, the fluorescence of **10**—$\lambda_{max} = 600$ and 652 nm, $\Phi = 0.04$, and $\tau = 2.4$ ns—resembles previously reported values.[23,31]

Upon the excitation of **12**, four emission bands at $\lambda = 649$ and 715 nm for H_2P and $\lambda = 600$ and 652 nm for ZnP are discernable in the fluorescence spectra. Nevertheless, the coalescence of the peaks at $\lambda = 649$ and 652 nm (i.e., H_2P and ZnP, respectively) is notable. The ZnP fluorescence is quenched by a factor of approximately 20, which corresponds to a lifetime of about 220 ps. Less pronounced is the impact in **12** on the H_2P fluorescence in which only a quenching of 50% is seen with a lifetime of about 5.76 ns in THF. Changing the solvent polarity from THF to either toluene or benzonitrile exerted a negligible impact on the fluorescence quantum yields and/or the fluorescence lifetimes (Table 2).

In the C_{60}-containing donor–acceptor conjugates **6** and **11**, the H_2P fluorescence is quantitatively quenched (i.e., >55-fold) without, however, affecting the overall shape of the fluorescence spectrum. In particular, the H_2P fluorescence quantum yields were in the range 2.0×10^{-3}–0.8×10^{-3}. Similarly, the ZnP unit in **11** has a negligible emission. For **6** and **11**, the fluorescence quantum yield and the fluorescence lifetime are subject to only a slight solvent dependence. No C_{60} fluorescence, which tends to be intrinsically weak (i.e., 6.0×10^{-4}) even in the C_{60} reference, was detectable at $\lambda = 720$ nm. A likely rationale implies that much stronger H_2P and ZnP fluorescence dominates this spectral region.

Table 2 summarizes the excited-state features of the donor–acceptor ensembles and the corresponding reference systems in solvents of varying polarity. Lifetimes, close to or below our detection limit, were estimated by using Equation (1).

$$k = \frac{\Phi_{Reference} - \Phi_{Compound}}{\tau_{Reference}\Phi_{Compound}} \quad (1)$$

Femtosecond flash photolysis: Ultrafast techniques were employed to characterize the transient intermediates involved in the excitation of **5**, **10**, **14**, **12**, **6**, and **11**. In particular, transient absorption spectroscopic measurements were carried out following femtosecond laser excitation at either $\lambda = 387$ or 420 nm in solvents of different polarity. The wavelength $\lambda = 387$ nm was used to photoexcite C_{60} nearly exclusively, whereas excitation at $\lambda = 420$ nm guarantees the excitation of ZnP or H_2P in the region of their Soret bands.

The photophysics of **14** is summarized as follows: the singlet excited state gives rise to a singlet–singlet absorption that maximizes around $\lambda = 920$ nm with a lowest vibronic state of 1.79 eV. Once generated, this state is subject to a rapid and quantitative intersystem crossing process to yield the energetically lower lying triplet excited state (1.50 eV).[32] The intersystem crossing takes place with a rate constant of $k = 7.4\times10^8\ s^{-1}$ and is governed by large spin–orbit coupling.[33] However, not only the rate is remarkable, the overall efficiency of the triplet formation is close to unity. The corresponding triplet excited-state features maxima in the visible region at $\lambda = 360$ and 720 nm (see Figure S1 in the Supporting Information).

Quite different are the differential absorption changes associated with the excitation of **5**. The visible region is dominated by intense H_2P-centered transitions that embrace minima due to ground-state bleaching at $\lambda = 516$, 549, 590, and 648 nm and maxima at $\lambda = 450$, 532, 567, 620, 674, and 1050 nm. Upon formation (i.e., >2 ps), intersystem crossing governs the photophysics of the singlet excited state (1.90 eV) of **5** over the course of approximately 10 ns. Similar to the H_2P singlet excited state, the ZnP singlet excited state forms within 1 ps. The singlet excited state displays a minimum—due to Q-band bleaching—at $\lambda = 550$ nm and maxima between $\lambda = 570$ and 740 nm and 900 and 1000 nm. Within 2.4 ns, the singlet excited state (2.04 eV) converts into the lower-lying triplet excited state (1.53 eV) through an efficient intersystem crossing in all measured solvents.[23,31,34]

The differential absorption changes that were recorded upon excitation of **12** (Figure 1) are dominated by the ZnP singlet excited-state features, whereas any appreciable contributions from the H_2P singlet excited state are insignificant. Within the next 140 ps, the ZnP singlet excited-state

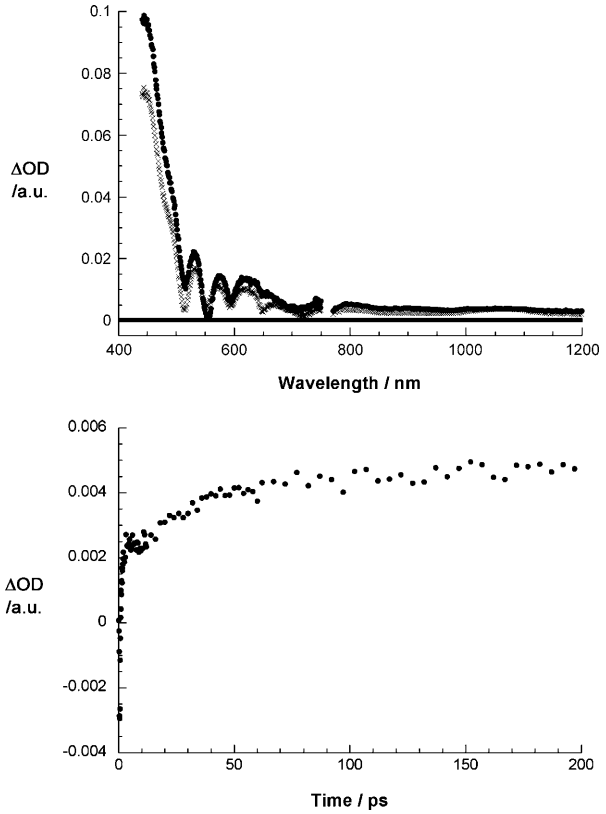

Figure 1. Upper: differential absorption spectra (visible and near-IR region) obtained upon femtosecond flash photolysis ($\lambda = 387$ nm) of **12** (10^{-4} M) in argon-saturated THF with time delays of 2 ps (filled circles) and 100 ps (crosses) at room temperature. Lower: time-absorption profile of the spectra shown above $\lambda = 553$ nm in which the energy transfer and the singlet-to-triplet intersystem crossing were monitored.

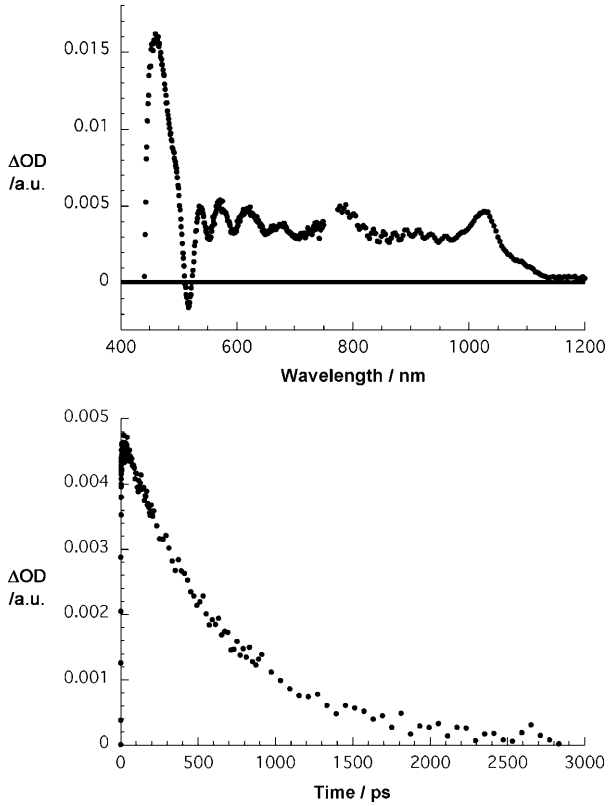

Figure 2. Upper: differential absorption spectrum (visible and near-IR region) obtained upon femtosecond flash photolysis ($\lambda = 387$ nm) of **6** (10^{-4} M) in argon-saturated THF with a time delay of 50 ps at room temperature. Lower: time-absorption profile of the spectra shown above $\lambda =$ 1040 nm, in which the charge separation and charge recombination were monitored.

(2.04 eV) features decay and simultaneously we see the H_2P singlet excited-state (1.9 eV) characteristics being formed. Implicit is a transduction of singlet excited-state energy driven along the energy gradient, the product of which starts to decay slowly on the timescale of the instrument, that is, 3 ns. It is notable that there is good agreement between the kinetic data derived from the transient absorption and the fluorescence measurements. Intersystem crossing (>3.0 ns), by which the H_2P singlet excited state is transformed into the corresponding triplet manifold, commences after the energy transfer.

The excited-state features of **6** (Figure 2) are dominated in the visible region by H_2P-centered transitions, whereas the excited-state properties of C_{60} are observed in the near-IR region. Instead of the slow intersystem crossing processes that both C_{60} and H_2P give rise to in the reference compounds, the C_{60}–H_2P excited state decays rapidly. In particular, after about 10 ps the growth of a characteristic absorption band in the near-IR region is discernable. A maximum at $\lambda = 1035$ nm is in perfect agreement with the fingerprint absorption of the C_{60} radical anion.[35] Simultaneously with the growth at $\lambda = 1035$ nm, a growth of a broad transient in the visible region (i.e., between $\lambda = 650$ and 700 nm) occurs. In comparison with the electrochemically and radiolytically generated features of the H_2P radical cation, we reach a conclusion with the successfully generated radical-ion-pair state $(C_{60})^{\bullet-}$-$(H_2P)^{\bullet+}$. With this information in hand, we derived the charge-separation (i.e., 60 ps, 1.6×10^{10} s^{-1}) and charge-recombination (i.e., 640 ps, 1.5×10^{9} s^{-1}) kinetics in THF. By increasing the solvent polarity, the driving forces for charge separation and recombination increase and decrease, thus obtaining lifetimes of 38 and 334 ps (2.6×10^{10} and 2.9×10^{9} s^{-1}, respectively) in benzonitrile.

In contrast to **6**, the photophysics of **11** follows a different deactivation pathway (Figure 3). Immediately upon photoexcitation in THF, the ZnP singlet excited-state features are discernable. These features convert rapidly ($k = 2.7\times10^{10}$ s^{-1}) into a new transient. Interestingly, the new transient is characteristic of the C_{60} radical anion that evolves in the near-IR region at $\lambda = 1035$ nm. Concurrently, the corresponding ZnP radical cation is registered in the visible range, namely, between $\lambda = 580$ and 800 nm. A spectral comparison with previous pulse radiolytic investigations on the one-electron oxidation of ZnP confirm the assignment of visible maxima to the $ZnP^{\bullet+}$ ion.[23,31] The $(C_{60})^{\bullet-}$-H_2P-$(ZnP)_3^{\bullet+}$ charge-separated state recombines in THF unexpectedly quickly ($k = 2.7\times10^{9}$ s^{-1}) and reinstates the singlet ground state (Table 3). The charge-separation and recombination processes reveal a

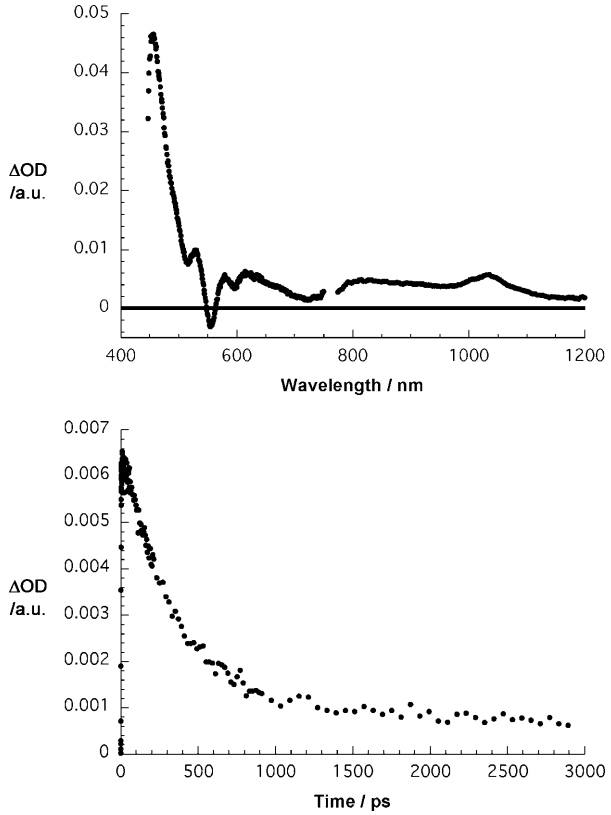

Figure 3. Upper: differential absorption spectrum (visible and near-IR region) obtained upon femtosecond flash photolysis ($\lambda = 387$ nm) of **11** (10^{-4} M) in argon-saturated THF with a time delay of 50 ps at room temperature. Lower: time-absorption profile of the spectra shown above $\lambda =$ 1040 nm, in which the charge separation and charge recombination were monitored.

Table 3. Charge-separation and charge-recombination kinetics for **11** and the corresponding driving forces[a] in different environments.

	CS I[b] [s^{-1}]	CS II[c] [s^{-1}]	CR [s^{-1}]	$-\Delta G^{o}_{CS}$ [eV]	$-\Delta G^{o}_{CR}$ [eV]
toluene	1.7×10^{10}		2.0×10^{9}	−0.11	2.15
THF	2.7×10^{10}		2.7×10^{9}	0.57	1.47
benzonitrile	8.3×10^{10}		1.0×10^{10}	0.79	1.25
toluene/pyridine (99:1 v/v)	9.8×10^{9}		1.3×10^{9}		
agar[d]		1.5×10^{9}	1.0×10^{7}		
Triton X-100[e]		9.3×10^{9}	2.1×10^{6}		

[a] The driving forces were estimated by using the dielectric continuum model (see the Supporting Information for details). [b] $(C_{60})^{\bullet-}$-H_2P-$(ZnP)_3^{\bullet+}$. [c] $(C_{60})^{\bullet-}$-$(H_2P)^{\bullet+}$-$(ZnP)_3$. [d] Agar (0.75 vol%) was added to an aqueous buffer solution (pH 7) and heated until the agar dissolved completely; after cooling to room temperature, a transparent jelly was formed; the compound, dissolved in Triton X-100, was added into the solution at 60 °C. [e] Degassed (Ar) Triton X-100.

weak solvent dependence with values of 59/489 ps (1.7×10^{10}/2.0×10^{9} s^{-1}) and 12/100 ps (8.3×10^{10}/1.0×10^{10} s^{-1}) in toluene and benzonitrile, respectively. However, no spectroscopic/kinetic evidence was found in favor of forming the $(C_{60})^{\bullet-}$-$(H_2P)^{\bullet+}$-$(ZnP)_3$ charge-separated state. Among several scenarios to explain this observation, two appear credible. The first scenario is based on thermodynamics, which suggest a larger driving force for the formation of $(C_{60})^{\bullet-}$-H_2P-$(ZnP)_3^{\bullet+}$ than for the formation of $(C_{60})^{\bullet-}$-$(H_2P)^{\bullet+}$-$(ZnP)_3$. The second is based on the nature of the linkers, due to their overall flexibility, which may facilitate a very close approach between the triad termini so that a direct charge separation between the C_{60} and ZnP units is feasible in a nonlinear assembly. In an effort to disrupt such potentially folded conformations of the triad, the addition of pyridine (i.e., 1% (v/v) in toluene) to coordinate the ZnP was investigated. The resulting spectrum was characterized by a redshift of 10 nm in absorption and a longer lived $(C_{60})^{\bullet-}$-H_2P-$(ZnP)_3^{\bullet+}$ species (i.e., 790 vs. 489 ps (1.3×10^{9} vs. 2.0×10^{9} s^{-1})) in pure toluene. The extended lifetime suggests that a strong perturbation of the distance and interactions between the C_{60} and ZnP units upon coordination of pyridine to the latter. However, the possible involvement of the $H_2P^{\bullet+}$ ion could not be confirmed.

Transient absorption measurements carried out after embedding **11** in an agar matrix led to drastic changes (Figure 4).[36] Under such experimental conditions, the ZnP

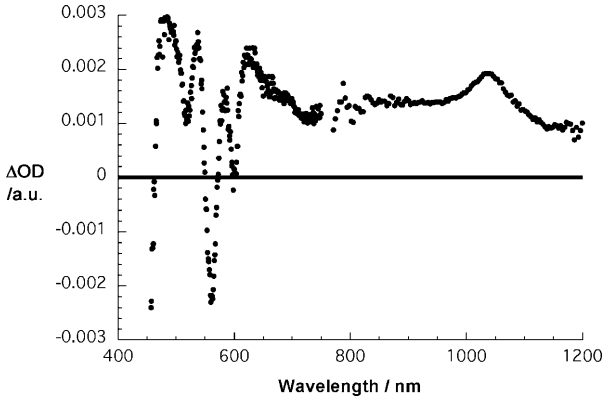

Figure 4. Differential absorption spectra (visible and near-IR region) obtained upon femtosecond flash photolysis ($\lambda = 387$ nm) of **11** (10^{-4} M) embedded in agar with a time delay of 100 ps at room temperature.

singlet excited-state features decay through energy transfer to afford the corresponding H_2P singlet excited state. The latter is then susceptible to charge transfer: the stable $(C_{60})^{\bullet-}$-$(H_2P)^{\bullet+}$-$(ZnP)_3$ radical-ion-pair state is seen within 657 ps (1.5×10^{9} s^{-1}) on the femtosecond scale. Complementary nanosecond experiments disclose a radical ion pair state with a lifetime of 100 ns (1.0×10^{7} s^{-1}; Figure 5). However, close examination indicates that it is not the $(C_{60})^{\bullet-}$-$(H_2P)^{\bullet+}$-$(ZnP)_3$ radical-ion-pair state that is observed in this case, but rather one corresponding to the $(C_{60})^{\bullet-}$-H_2P-$(ZnP)_3^{\bullet+}$. This result indicates a cascade of charge-transfer reactions that convert the initially formed $(C_{60})^{\bullet-}$-$(H_2P)^{\bullet+}$-$(ZnP)_3$ into $(C_{60})^{\bullet-}$-H_2P-$(ZnP)_3^{\bullet+}$. The underlying charge-shift reaction must have taken place on a timescale between 3 and 10 ns (i.e., the time resolution of the femtosecond and nanosecond setups, respectively).

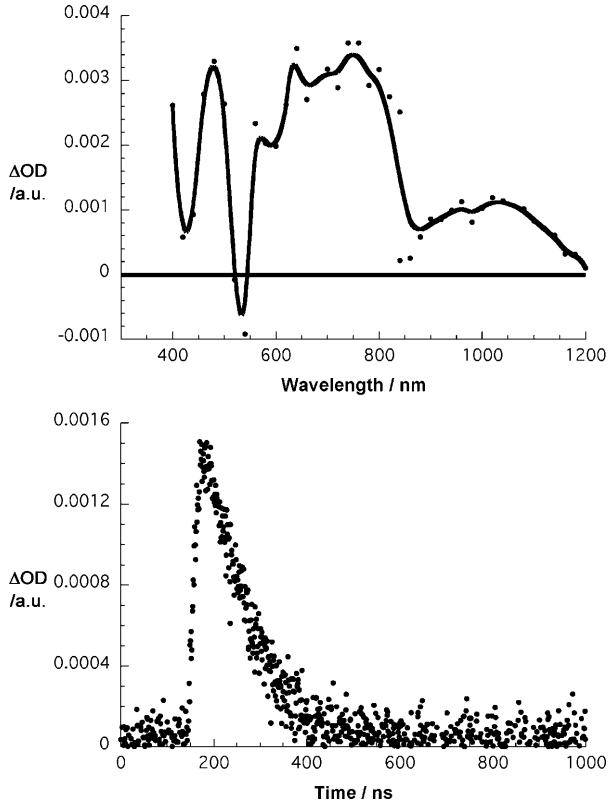

Figure 5. Upper: differential absorption spectra (visible and near-IR region) obtained upon nanosecond flash photolysis ($\lambda = 355$ nm) of **11** (10^{-4} M) embedded in agar with a time delay of 200 ns at room temperature. Lower: time-absorption profile of the spectra shown above $\lambda =$ 1040 nm, in which the charge recombination was monitored.

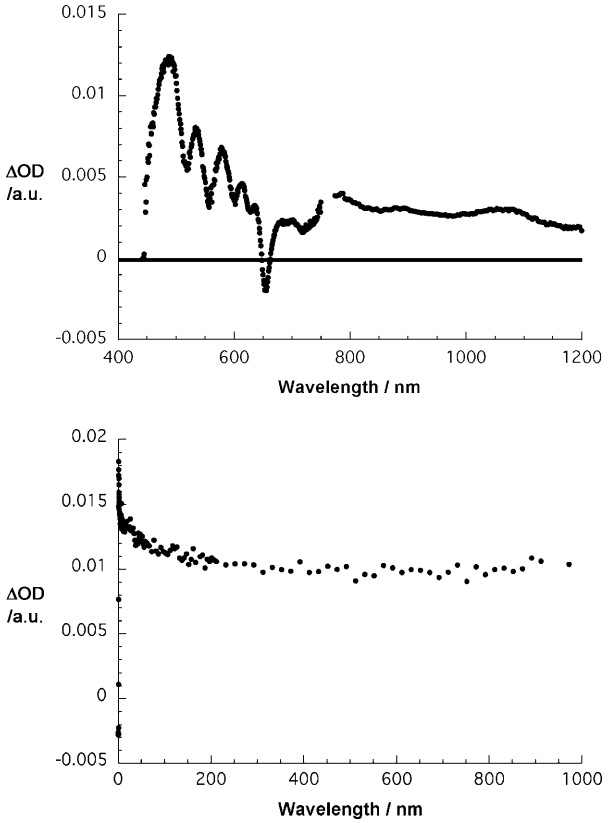

Figure 6. Upper: differential absorption spectrum (visible and near-IR region) obtained upon femtosecond flash photolysis ($\lambda = 387$ nm) of **11** in argon-saturated Triton X-100 with a time delay of 200 ps at room temperature. Lower: time-absorption profile of the spectra shown above $\lambda =$ 475 nm, in which the charge separation and charge recombination were monitored.

An even more efficient and longer lived charge separation was observed in pure Triton X-100 (viscosity = 240 cP; Figure 6). Under such experimental conditions, the ZnP singlet excited-state features decay through energy transfer to afford the corresponding H_2P singlet excited state. The charge separation occurred in the triad to form $H_2P^{\bullet+}$-$C_{60}^{\bullet-}$ out of the H_2P singlet excited state within 107 ps. The recovery of the ground state evolving from the intermediate $ZnP^{\bullet+}$-$C_{60}^{\bullet-}$ charge-separated state takes place with $k = 2.1 \times 10^6$ s^{-1}. Again, the charge migration was not observable due to our instrumental response.

Energetics: The photoexcited **12** deactivates through the following sequence of processes: the initially-formed ZnP (2.04 eV) singlet excited state deactivates by an exothermic energy transfer (0.15 eV) to the H_2P singlet excited state (1.9 eV). This process is followed by intersystem crossing to the H_2P triplet excited state (1.40 eV) and the subsequent recovery of the ground state.

The energy of the $(H_2P)^{\bullet-}$–$(ZnP)_3^{\bullet+}$ radical-ion-pair state is 2.09 eV in THF, which makes it impossible to be formed from any of the singlet excited states. Increasing the solvent polarity also (e.g., with benzonitrile) increases the driving force for charge separation to 0.19 and 0.04 eV when considering the ZnP and H_2P singlet excited states, respectively. Nevertheless, energy transfer outperforms the formation of the radical-ion-pair state.

The low C_{60} reduction potential changes the deactivation pathways drastically in **6**. Taking, for example, the driving force for charge separation, which increases in THF to 0.30 eV, the charge recombination is strongly exothermic with 1.59 eV. Here, the recombination to form the triplet excited state is 0.19 eV more favorable than the direct recovery of the ground state. When increasing the solvent polarity to benzonitrile, the energy of the radical-ion-pair state (1.43 eV) approached that of the H_2P triplet excited state. As a matter of fact, deactivation proceeds predominantly to the ground state. Even in toluene, there was evidence for charge separation, although the dielectric continuum model suggests that this process should be endothermic, namely, energetically uphill by 0.17 eV. It is likely that the calculated value is an overestimation, especially considering that the charge transfer proceeds through a nonlinear assembly and that, in turn, a correct distance is difficult to approximate.

Turning to **11**, several deactivation scenarios emerge. Firstly, a unidirectional energy transfer by 0.15 eV, with close resemblance to the aforementioned **12**. Secondly,

direct charge separation to afford $(C_{60})^{\bullet-}$-H_2P-$(ZnP)_3^{\bullet+}$, which is exothermic by 0.57 eV. Both processes are fairly efficient and, thus, fluorescence or intersystem crossing, as intrinsic deactivation processes, are nearly quantitatively shut down. The flexibility of the linker enables a competitive scenario, in which the charge recombination surpasses the energy transfer (Figure 7). From this point, the only feasible process is the recovery of the ground state. By enforcing a more linear configuration of **11**—through the choice of a highly viscous solvent or a matrix—eliminates the charge transfer, and instead we note the transduction of singlet excited-state energy as the major deactivation. The correspondingly formed C_{60}-*(H_2P)-$(ZnP)_3$ is subject to charge separation and charge shift to yield $(C_{60})^{\bullet-}$-$(H_2P)^{\bullet+}$-$(ZnP)_3$ and $(C_{60})^{\bullet-}$-H_2P-$(ZnP)_3^{\bullet+}$, respectively.

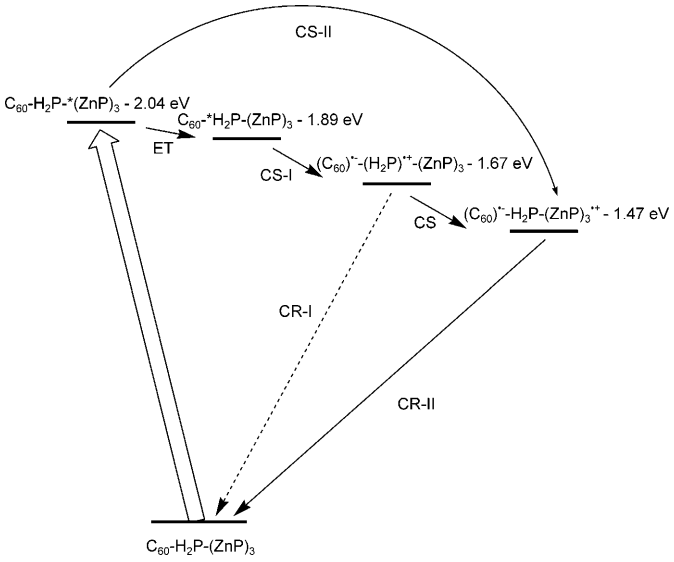

Figure 7. Energy diagram that illustrates the deactivation pathways in photoexcited **11** in agar/Triton X-100 (i.e., energy transfer from C_{60}-H_2P-*$(ZnP)_3$ to C_{60}-*H_2P-$(ZnP)_3$ (ET), formation of $(C_{60})^{\bullet-}$-$(H_2P)^{\bullet+}$-$(ZnP)_3$ (CS-I), followed by a charge-shift reaction to form $(C_{60})^{\bullet-}$-H_2P-$(ZnP)_3^{\bullet+}$ (CS), and charge recombination to the ground state (CR-2)) and in, for example, THF (i.e., direct formation of $(C_{60})^{\bullet-}$-H_2P-$(ZnP)_3^{\bullet+}$ (CS-II) and charge recombination to the ground state (CR-II)). Charge recombination (CR-I) from the intermediately formed $(C_{60})^{\bullet-}$-$(H_2P)^{\bullet+}$-$(ZnP)_3$ has also been added.

Conclusions

In summary, we have demonstrated unequivocally herein light harvesting, unidirectional energy transfer, charge transfer, and charge shift in a single donor–acceptor conjugate, C_{60}-H_2P-$(ZnP)_3$. The dendritic architecture built with driving forces for all of the aforementioned processes is important in this context. Owing, however, to the flexibility of the linkers, which connect the C_{60}, H_2P, and ZnP, the outcome of photoexcitation depends strongly on environmental influences on the conformation. In Triton X-100 or an agar matrix, time-resolved transient absorption spectroscopy and fluorescence lifetime measurements confirm the formation of $(C_{60})^{\bullet-}$-H_2P-$(ZnP)_3^{\bullet+}$ with lifetimes of 100 and 460 ns, respectively. On the other hand, investigations in organic media (i.e., toluene, THF, and benzonitrile) trigger substantial configurational rearrangements, which place ZnP and C_{60} units in proximity to each other. Consequently, the lifetime of $(C_{60})^{\bullet-}$-H_2P-$(ZnP)_3^{\bullet+}$ is as short as 100 ps in benzonitrile. Implicit is that in Triton X-100/agar matrix a stretched configuration seems to be favored for C_{60}-H_2P-$(ZnP)_3$ by altering the conformational equilibrium of the system, whereas in organic media coiling up of C_{60}-H_2P-$(ZnP)_3$ results through space π–π/charge-transfer interactions between ZnP and C_{60}. An alternative rationale implies that in Triton X-100/agar matrix the motions needed for ZnP quenching by charge transfer are not competitive with those for the corresponding energy-transfer reaction. Our current efforts are directed to the implementation of a rigid spacer that 1) prevents structural rearrangement; 2) provides the necessary electronic coupling to power light harvesting, unidirectional energy transfer, charge transfer, and charge-shift reactions; and 3) slows down the energy-wasting charge recombination.

Experimental Section

General: Fullerene C_{60} was obtained from Hoechst AG/Aventis and separated from higher fullerenes by plug filtration.[37] Solvents were purified by distillation, or in the case of HPLC grade solvents, used as received. All the solvents employed for the electrochemical, photochemical, and photophysical investigations were purchased from chemical suppliers in dry, spectroscopic grade and were used without further purification. TLC analysis was carried out on Merck silica gel 60 F_{254}. Column chromatography was performed on Macherey–Nagel silica gel 60 M (230–400 mesh, 0.04–0.063 mm). The FAB mass spectra were recorded on a Micromass Zabspec FAB+ mode with 3-nitrobenzyl alcohol as the matrix. The MALDI-TOF mass spectra were carried out on a Shimadzu Axima Confidence (DCTB: *trans*-2-[3-(4-*tert*-butylphenyl)-2-methyl-2-propenylidene]malononitrile, DITH: dithranol, SIN: sinaptic acid). The ESI mass spectra were obtained on a Bruker Esquire 6000 spectrometer and the EI mass spectra were recorded on a Varian MAT 311A spectrometer. The NMR spectra were recorded on Jeol (Jeol JNM EX 400, Jeol JNM GX 400) and Bruker (Bruker Avance 300, Bruker Avance 400) spectrometers. The measurements were carried out in $CDCl_3$ and $[D_8]$THF, which were used as standards (solvent peaks in ^1H and ^{13}C NMR spectra: $CDCl_3$: $\delta = 7.24$ and 77.00 ppm, $[D_8]$THF: $\delta = 3.58$ and 67.57 ppm). The elemental analysis was obtained by using a CE Instruments Elemental Analyzer 1110 CHNS machine. UV/Vis spectroscopic analysis was performed on SPECORD S600, Analytik Jena AG, and Varian Cary 5000 UV/Vis/NIR spectrophotometers. The absorption maxima λ_{max} are given in nm. IR spectroscopic analysis was carried out on Reakt-IR 1000 Asi Applied Systems, ATR DiComp detector, and ThermoScientific Nicolet IR100 FT-IR spectrophotometers. The electrochemical experiments were carried out using a BAS-CV50W electrochemical workstation with positive feedback compensation. Cyclic, differential-pulse, and square-wave voltammetry were performed in a three-electrode cell with a platinum wire as the counterelectrode, a glassy carbon disk as the working electrode ($\varnothing = 2$ mm) versus a silver wire as the reference electrode; ferrocene was applied as an internal standard and a 0.1 M solution of $(t\mathrm{Bu})_4NBF_4$ as the supporting electrolyte. All the experiments were performed in an inert gas atmosphere and at a compound concentration of 0.2 mM. Steady-state fluorescence spectroscopic analysis was performed on a Horiba Jobin Yvon Fluoromax 3 spectrophotometer. Deaerated solutions at room tem-

perature (298 K) in a 1-cm quartz cuvette were used. All the spectra were corrected for the instrument response. The monitoring wavelength corresponded to the maximum of the emission band. For excitation wavelengths below $\lambda = 450$ nm a cut-off filter (450 nm) was inserted. In the time-resolved fluorescence experiments, the fluorescence lifetime measurements were performed on a SPEX Fluorolog-3 (HORIBA-JOBIN YVON) machine supplied with an integrated TCSPC software. The wavelength of $\lambda = 403$ nm was selected as the excitation wavelength for the lifetime measurements (nano-LED-403L; pulse width: < 100 ps). The fluorescence lifetimes were measured at the emission maximum at room temperature in deaerated solutions in a 1 to 1-cm quartz cuvette. Femtosecond transient absorption studies were performed with 387-nm laser pulses (1 kHz, pulse width: 150 fs, 200 nJ) from an amplified Ti/sapphire laser system (Model CPA 2010, Clark-MXR Inc.; output: 775 nm). For an excitation wavelength of 420 nm, a nonlinear optical parametric converter (NOPA) was used to generate ultrashort tunable visible pulses out of the pump pulses. The transient absorption pump probe spectrometer (TAPPS) is referred to as a two-beam setup, in which the pump pulse is used as an excitation source for transient species and the delay of the probe pulse is exactly controlled by an optical delay rail. As a probe (white-light continuum), a small fraction of pulses that stem from the CPA laser system was focused by a 50-mm lens into a sapphire disc (thickness: 5 mm). The transient spectra were recorded using fresh oxygen-free solutions in each laser excitation. All the experiments were performed at 298 K in a 2-mm quartz cuvette. Transient absorption experiments, based on nanosecond laser photolysis, were performed with the output of the third harmonics (355 nm) coming from a Nd/YAG laser (Brilliant, Quantel). Moreover, pulse widths of < 5 ns with an energy of 10 mJ were selected. The optical detection is based on a pulsed Xenon lamp (XBO 450, Osram), a monochromator (Spectra Pro 2300i, Acton Research), a R928 photomultiplier tube (Hamamatsu Photonics), or a fast InGaAs photodiode (Nano 5, Coherent) with amplification of 500 MHz and a digital oscilloscope (1 GHz; WavePro7100, LeCroy). The laser power of every laser pulse was registered by using a bypath with a fast silicon photodiode. The nanosecond laser photolysis experiments were performed with 1-cm quartz cells and the solutions were saturated with argon if no other gas saturation is indicated.

***tert*-Butyl 2-(3-formylphenoxy)acetate (3)**: 3-(2-Hydroxyethoxy)benzaldehyde (16.00 g, 130.0 mmol), *tert*-butyl bromoacetate (20 mL, 137.2 mmol), and tetrabutylammonium bromide (4.40 g, 14.0 mmol) dissolved in CH_2Cl_2 (100 mL) were added to NaOH (5.20 g, 130.0 mmol) in H_2O (100 mL). The reaction mixture was stirred for 16 h at room temperature. The organic phase was separated, the aqueous phase was washed four times with CH_2Cl_2, and the solvent was removed from the combined organic phases. The resulting yellow oil was mixed with water and subsequently extracted with diethyl ether. This organic phase was washed twice with 2 N NaOH, dried over $MgSO_4$, and the solvent was distilled off (30.08 g, 127.00 mmol, 97%). ^{1}H NMR (400 MHz, $CDCl_3$, RT): $\delta = 9.94$ (s, 1H; CHO), 7.49–7.47, 7.47–7.44, 7.44–7.42, 7.42–7.41, 7.33–7.30, 7.21–7.19, 7.19–7.17 (m, 4H; Ar-H), 4.56 (s, 2H; CH_2), 1.46 ppm (s, 9H; CH_3); ^{13}C NMR (100 MHz, $CDCl_3$, RT): $\delta = 191.79$ (CHO), 167.46 (*C*OO), 158.44, 137.72, 130.18, 124.26, 122.01, 112.68 (Ar-C), 82.70 (*C*CH_3), 65.59 (CH_2), 27.98 ppm (C*C*H_3); IR: $\tilde{\nu} = 3011$, 2984, 2945, 2833, 2744, 1741, 1695, 1594, 1482, 1459, 1393, 1370, 1328, 1282, 1227, 1146, 1073, 1038, 996, 977, 953, 923, 869, 845, 787, 733, 679 cm^{-1}; EI-MS: m/z: 236 [M^+], 180 [$M^+ - t$Bu].

1′-Methoxycarbonyl-1′-{2-[3-(5-{10,15,20-tris[3-(hydrogencarboxymethoxy)phenyl]porphyrin})]phenoxy}ethoxycarbonyl-1,2-methano-[60]fullerene (7): Dyad **6** (205 mg, 0.12 mmol) was added to formic acid (40 mL). After stirring overnight, the formic acid was distilled off. Toluene was added and evaporated several times for purification (quantitative yield). ^{1}H NMR (300 MHz, [D_8]THF, RT): $\delta = 8.95$–8.65 (m, 8H; β-pyrr-H), 8.10–7.53, 7.45–7.28 (m, 16H; Ar-H), 4.86 (s, 2H; CH_2), 4.81 (s, 4H; CH_2), 4.71 (s, 2H; CH_2), 4.46 (s, 2H; CH_2), 3.93 (s, 3H; OCH_3), −2.91 ppm (s, 2H; NH); ^{13}C NMR (75 MHz, [D_8]THF, RT): $\delta = 170.57$, 170.52, 170.43, 170.34 (COOH), 164.07, 163.67 (*COCCO*), 158.21, 158.07, 158.01, 157.91 (Ar-C), 145.88, 145.34, 145.03, 144.82, 144.79, 144.55, 144.50, 144.46, 143.96, 143.66, 142.90, 142.64, 142.39, 142.02, 141.92, 141.64, 141.55, 141.27, 141.15, 140.36, 140.26, 139.72, 138.59, 138.49 (Ar-C, C_{60}), 131.96 (β-pyrr-C), 129.07, 128.75, 128.66, 128.56, 128.22 (Ar-C), 121.80, 121.66, 121.50, 121.35, 121.20, 121.15, 121.08, 120.77, 120.74 (Ar-C, *meso*-C), 115.94, 115.86, 115.79, 115.73, 115.54 (Ar-C), 72.11 (C_{60} sp^3), 66.16, 65.74, 65.67, 65.58, 65.52 (CH_2), 54.37 (OCH_3), 53.04 ppm (CO*C*CO); IR: $\tilde{\nu} = 2359$, 2340, 1726, 1574, 1471, 1426, 1229, 1163, 1058, 976, 912, 799, 775, 726, 695, 637, 578, 551, 524, 462, 428 cm^{-1}; UV/Vis (THF): λ_{max} (ε) = 257 (120000), 327 (46800), 427 (195000), 517 (14200), 551 (7200), 595 (4900), 650 nm (3000 M^{-1}cm^{-1}); MALDI-TOF-MS (DCTB): m/z: 1716 [M^++H].

Dendritic porphyrin–fullerene hybrid C_{60}-H_2P-(ZnP)$_3$ (11): Dyad **7** (91 mg, 53 μmol), DMAP (8 mg, 64 μmol), and HOBT (28 mg, 207 μmol) were dissolved in dry THF (15 mL) under nitrogen. The solution was cooled to 0 °C and light was excluded. DCC (43 mg, 207 μmol) was added with stirring. After 10 min at 0 °C, porphyrin **10** (117 mg, 159 μmol) was added to the reaction mixture, which was stirred for 20 min at 0 °C and 6 days at ambient temperature. At 0 °C, DCC (62 mg, 300 μmol) was added and stirred for 1 day at ambient temperature. The solvent was removed and the residue was redissolved in CH_2Cl_2 then filtered through Celite 500. The product was purified by column chromatography (silica gel, CH_2Cl_2/EtOAc 20:0.75, 1% NEt_3, without sand on top) and recrystallized from CH_2Cl_2/pentane (86 mg, 22 μmol, 42% relative to **10**). ^{1}H NMR (400 MHz, $CDCl_3$, RT): $\delta = 9.00$–8.50 (m, 32H; β-pyrr-H), 8.30–6.80 (m, 73H; Ar-H), 4.75–3.60 (m, 25H; CH_2, CH_3), −3.17 ppm (s, 2H; NH); ^{1}H NMR (400 MHz, $C_2D_2Cl_4$, 100 °C): $\delta = 9.00$–8.55 (m, 32H; β-pyrr-H), 8.30–7.10 (m, 73H; Ar-H), 4.90–4.10 (m, 22H; CH_2), 4.00–3.75 (m, 3H; OCH_3), −2.88 ppm (s, 2H; NH); ^{13}C NMR (100 MHz, $CDCl_3$, RT): $\delta = 168.63$, 168.55, 168.49, 168.42, 168.33, 168.31, 168.25, 168.21, 168.10, 168.00 (CO), 163.15, 163.00, 162.96, 162.87, 162.79, 162.72 (CO malonyl), 156.44, 156.39, 156.31, 156.19, 156.00, 155.92, 155.85, 155.73, 155.65, 155.56 (Ar-C), 150.13, 149.90 (α-pyrr-C), 144.25, 144.22, 144.19, 144.12, 144.06, 143.43, 143.40, 143.29, 142.75, 142.69 (Ar-C), 142.55, 142.36, 142.30, 142.22, 142.11, 142.05, 141.95, 141.88, 141.80, 141.70, 141.65, 141.56, 141.52, 141.41, 141.34, 141.19, 141.14, 140.79, 140.62, 140.46, 140.44, 140.33, 140.27, 140.14, 140.01, 139.87, 139.83, 139.52, 139.27, 139.19, 139.14, 139.04, 138.86, 138.78, 138.57, 138.52, 138.46, 138.32, 138.14, 138.04, 137.92, 137.80, 137.70, 137.64, 137.54, 137.45, 136.46, 136.33, 136.25 (C_{60}, Ar-C), 134.33 (Ar-C), 131.97, 131.80, 131.00 (β-pyrr-C), 128.38, 128.17, 127.94, 127.75, 127.65, 127.60, 127.39, 126.48 (Ar-C), 123.62, 121.18, 121.12, 120.91, 120.76, 120.39, 119.97, 119.89, 119.72, 119.52, 119.49, 119.40 (Ar-C, *meso*-C), 115.32, 115.28, 114.89, 114.80, 114.48, 114.40, 114.26, 113.95, 113.82 (Ar-C), 69.87, 69.75 (C_{60} sp^3), 67.18, 67.10, 65.66, 65.54, 65.48, 65.41, 65.21, 65.07, 65.00, 64.76, 63.45, 63.30, 63.23, 62.98 (CH_2), 53.74, 53.72, 53.68 (OCH_3), 50.83, 50.78, 50.74, 50.70 ppm ($C_{quart.}$ malonyl); ^{13}C NMR (100 MHz, $C_2D_2Cl_4$, 100 °C): $\delta =$ 168.82, 168.78 (CO), 163.43, 163.17 (CO malonyl), 157.11, 157.02, 156.73, 156.66 (Ar-C), 150.63, 150.42, 146.96, 146.90 (α-pyrr-C), 144.64, 144.26, 143.93, 143.85, 143.72, 143.13, 142.63, 142.61, 142.55, 142.40, 141.72, 141.67, 141.61, 141.57, 141.50, 141.27, 141.22, 140.60, 140.34, 139.92, 139.63, 139.16, 138.91, 138.84, 138.76, 138.66, 138.14, 138.07, 137.32, 137.20, 137.16 (C_{60}, Ar-C), 134.75 (Ar-C), 132.32, 132.24, 132.11, 131.31 (β-pyrr-C), 128.82, 128.47, 128.29, 128.04, 127.95, 127.74, 126.79 (Ar-C), 121.87, 121.74, 121.57, 121.51, 120.77, 119.91, 119.88, 119.81 (Ar-C, *meso*-C), 115.80, 114.99 (Ar-C), 70.77 (C_{60} sp^3), 67.77, 66.50, 66.09, 66.04, 65.25, 63.71 (CH_2), 53.84 ppm (OCH_3); IR: $\tilde{\nu} = 1749$, 1596, 1576, 1481, 1438, 1339, 1286, 1233, 1174, 1069, 1002, 995, 913, 795, 754, 729, 718, 700, 660, 580, 525, 460, 433, 406 cm^{-1}; UV/Vis (CH_2Cl_2): λ_{max} (ε) = 259 (160400), 420 (1053000), 517 (20700), 549 (54500), 589 nm (13100 M^{-1}cm^{-1}); MALDI-TOF-MS (DCTB): m/z: 3875 [M^++H]; ESI-MS (CH_2Cl_2): m/z: 1937.3 [M^{2+}], 1291.5 [M^{3+}], 968.9 [M^{4+}].

Dendritic porphyrin H_2P-(ZnP)$_3$ (12): Porphyrin **13** (59 mg, 59 μmol), DMAP (9 mg, 70 μmol), and HOBT (31 mg, 229 μmol) were dissolved in dry THF (15 mL) under nitrogen. The solution was cooled to 0 °C and light was excluded. DCC (47 mg, 229 μmol) was added to the reaction mixture with stirring. After 5 min, porphyrin **10** (130 mg, 176 μmol) was added to the reaction mixture, which was stirred for 20 min at 0 °C and 5 days at ambient temperature. The solvent was removed and the residue was redissolved in CH_2Cl_2 then filtered. The product was purified by column chromatography (silica, CH_2Cl_2/EtOAc 20:0.75, 1% NEt_3, without sand on top) and recrystallized from CH_2Cl_2/pentane (81 mg,

25.65 μmol, 44% relative **13**). ^{1}H NMR (400 MHz, $CDCl_3$, RT): δ = 9.10–8.75 (m, 32H; β-pyrr-H), 8.40–8.10 (m, 18H; Ar-H), 7.90–6.65 (m, 55H; Ar-H), 4.80–3.80 (m, 22H; CH_2, CH_3), 3.65–3.35 (m, 3H; CH_2, CH_3), 3.25–2.80 (m, 2H; CH_2, CH_3), −2.74 ppm (s, 2H; NH); ^{1}H NMR (400 MHz, $C_2D_2Cl_4$, 100 °C): δ = 9.20–8.80 (m, 32H; β-pyrr-H), 8.50–8.00 (m, 18H; Ar-H), 8.00–6.70 (m, 55H; Ar-H), 5.00–4.10 (m, 22H; CH_2), 3.80–3.50 (s, 3H; OCH_3), 3.40–3.20 (m, 2H; CH_2), −2.59 ppm (s, 2H; NH); ^{13}C NMR (100 MHz, $CDCl_3$, RT): δ = 168.64, 168.53, 168.47, 168.39 (CO), 166.56, 166.42, 166.30, 166.14, 166.04 (CO malonyl), 156.56, 156.39, 156.35, 156.25, 155.99, 155.93, 155.87 (Ar-C), 150.17, 149.93 (α-pyrr-C), 144.12, 144.07, 143.99, 143.41, 143.32, 142.75, 142.68, 134.38, 134.33 (Ar-C), 132.01, 131.84, 131.20 (β-pyrr-C), 128.56, 128.10, 127.96, 127.90, 127.56, 127.51, 127.42, 127.37, 127.18, 126.49, 126.44 (Ar-C), 121.22, 121.13, 120.89, 120.40, 119.67, 119.50 (Ar-C, *meso*-C), 114.15, 113.79 (Ar-C), 65.67, 65.57, 65.11, 65.02, 63.62, 63.41, 63.28, 63.16 (CH_2), 52.37, 52.30, 52.23 (OCH_3), 40.83, 40.77, 40.62, 40.58, 40.44, 40.40 ppm ($C_{quart.}$ malonyl); ^{13}C NMR (100 MHz, $C_2D_2Cl_4$, 100 °C): δ = 168.98, 168.94 (CO), 166.71, 166.44 (CO malonyl), 157.36, 157.20, 156.88 (Ar-C), 150.69, 150.47, 147.03 (α-pyrr-C), 144.63, 143.94, 143.13, 134.78 (Ar-C), 132.30, 132.15, 131.41 (β-pyrr-C), 129.07, 128.64, 127.90, 127.77, 127.66, 126.78 (Ar-C), 122.10, 121.59, 121.51, 120.78, 120.06, 119.86 (Ar-C, *meso*-C), 114.98, 114.87, 114.79 (Ar-C), 66.69, 66.26, 63.92, 63.84 (CH_2), 52.39 (OCH_3), 41.17 ppm ($C_{quart.}$ malonyl); IR: $\tilde{\nu}$ = 1595, 1574, 1478, 1437, 1337, 1277, 1159, 1067, 993, 908, 793, 752, 717, 698, 658, 587, 566, 514, 503, 484, 466, 433, 413 cm^{-1}; UV/Vis (CH_2Cl_2): λ_{max} (ε) = 418 (1419000), 515 (26000), 549 (68000), 588 nm (14400 $M^{-1}cm^{-1}$); MALDI-TOF-MS (DCTB): *m/z*: 3156 [M^++H]; ESI-MS (CH_2Cl_2): *m/z*: 1577.9 [M^{2+}], 1052.0 [M^{3+}], 789.37 [M^{4+}].

Acknowledgements

Financial support from the German Science Foundation (DFG) through SFB 583 is gratefully acknowledged. G.K. acknowledges NSF IGERT: Materials Creation Training Program (MCTP) (DGE-0654431).

[1] J. Deisenhofer, H. Michel, *Angew. Chem.* **1989**, *101*, 872; *Angew. Chem. Int. Ed. Engl.* **1989**, *28*, 829.
[2] J. Deisenhofer, J. R. Norris in *The Photosynthetic Reaction Center*, Academic Press, New York, **1993**.
[3] D. Gust, T. A. Moore, A. L. Moore, *Acc. Chem. Res.* **1993**, *26*, 198–205.
[4] T. Asahi, M. Ohkouchi, R. Matsusaka, N. Mataga, R. P. Zhang, A. Osuka, K. J. Maruyama, *J. Am. Chem. Soc.* **1993**, *115*, 5665–5674.
[5] Y. Sakata, H. Imahori, H. Tsue, S. Higashida, T. Akiyama, E. Yoshizawa, M. Aoki, K. Yamada, K. Hagiwara, S. Taniguchi, T. Okada, *Pure Appl. Chem.* **1997**, *69*, 1951–1956.
[6] M. R. Wasielewski, *Chem. Rev.* **1992**, *92*, 435–461.
[7] E. Dietel, A. Hirsch, E. Eichhorn, A. Rieker, S. Hackbarth, B. Roeder, *Chem. Commun.* **1998**, 1981–1982.
[8] D. M. Guldi, C. Luo, M. Prato, E. Dietel, A. Hirsch, *Chem. Commun.* **2000**, 373–374.
[9] D. M. Guldi, C. Luo, T. da Ros, M. Prato, E. Dietel, A. Hirsch, *Chem. Commun.* **2000**, 375–376.
[10] D. M. Guldi, C. Luo, M. Prato, A. Troisi, F. Zerbetto, M. Scheloske, E. Dietel, W. Bauer, A. Hirsch, *J. Am. Chem. Soc.* **2001**, *123*, 9166–9167.
[11] D. M. Guldi, C. Luo, A. Swartz, M. Scheloske, A. Hirsch, *Chem. Commun.* **2001**, 1066–1067.
[12] D. M. Guldi, A. Hirsch, M. Scheloske, E. Dietel, A. Troisi, F. Zerbetto, M. Prato, *Chem. Eur. J.* **2003**, *9*, 4968–4979.
[13] H. Imahori, D. M. Guldi, K. Tamaki, Y. Yoshida, C. Luo, Y. Sakata, S. Fukuzumi, *J. Am. Chem. Soc.* **2001**, *123*, 6617–6628.
[14] H. Imahori, N. V. Tkachenko, V. Vehmanen, K. Tamaki, H. Lemmetyinen, Y. Sakata, S. Fukuzumi, *J. Phys. Chem. A* **2001**, *105*, 1750–1756.
[15] V. Chukharev, N. Tkachenko, A. Efimov, D. M. Guldi, A. Hirsch, M. Scheloske, H. Lemmetyinen, *J. Phys. Chem. B* **2004**, *108*, 16377–16385.
[16] D. Gust, T. A. Moore, A. L. Moore, *Acc. Chem. Res.* **2001**, *34*, 40–48.
[17] L. Echegoyen, L. E. Echegoyen, *Acc. Chem. Res.* **1998**, *31*, 593.
[18] Q. Xie, E. Perez-Cordero, L. Echegoyen, *J. Am. Chem. Soc.* **1992**, *114*, 3978.
[19] H. Imahori, K. Hagiwara, T. Akiyama, M. Aoki, S. Taniguchi, T. Okada, M. Shirakawa, Y. Sakata, *Chem. Phys. Lett.* **1996**, *263*, 545.
[20] G. McDermott, S. M. Prince, A. A. Freer, A. M. Hawthornthwaite-Lawiess, M. Z. Papiz, R. J. Cogdell, N. W. Isaacs, *Nature* **1995**, *374*, 517–521.
[21] F. Spänig, C. Kovacs, F. Hauke, K. Ohkubo, S. Fukuzumi, D. M. Guldi, A. Hirsch, *J. Am. Chem. Soc.* **2009**, *131*, 8180–8195.
[22] A. McKillop, J.-C. Fiaud, R. P. Hug, *Tetrahedron* **1974**, *30*, 1379–1382.
[23] D. M. Guldi, A. Hirsch, M. Scheloske, E. Dietel, A. Troisi, F. Zerbetto, M. Prato, *Chem. Eur. J.* **2003**, *9*, 4968–4979.
[24] a) G. R. Geier III, B. J. Littler, J. S. Lindsey, *J. Chem. Soc. Perkin Trans. 2* **2001**, 712–718; b) J. S. Lindsey, I. C. Schreiman, H. C. Hsu, P. C. Kearney, A. M. Maguerettaz, *J. Org. Chem.* **1987**, *52*, 827–836; c) J. S. Lindsey, R. W. Wagner, *J. Org. Chem.* **1989**, *54*, 828–836; d) J. S. Lindsey, K. A. MacCrum, J. S. Tyhonas, Y.-Y. Chuang, *J. Org. Chem.* **1994**, *59*, 579–587; e) F. Li, K. Yang, J. S. Tyhonas, K. A. MacCrum, J. S. Lindsey, *Tetrahedron* **1997**, *53*, 12339–12360.
[25] a) C. Bingel, *Chem. Ber.* **1993**, *126*, 1957–1959; b) J.-F. Nierengarten, V. Gramlich, F. Cardullo, F. Diederich, *Angew. Chem.* **1996**, *108*, 2242–2244; *Angew. Chem. Int. Ed. Engl.* **1996**, *35*, 2101–2103.
[26] C. Kovacs, A. Hirsch, *Eur. J. Org. Chem.* **2006**, 3348–3357.
[27] M. Brettreich, S. Burghardt, C. Böttcher, T. Bayerl, S. Bayerl, A. Hirsch, *Angew. Chem.* **2000**, *112*, 1915; *Angew. Chem. Int. Ed.* **2000**, *39*, 1845.
[28] D. Kuciauskas, S. Lin, G. R. Seely, A. L. Moore, T. A. Moore, D. Gust, T. Drovetskaya, C. A. Reed, P. D. W. Boyd, *J. Phys. Chem.* **1996**, *100*, 15926.
[29] W. A. Lee, M. Graetzel, K. Kalyanasundaram, *Chem. Phys. Lett.* **1984**, *107*, 308.
[30] K. Tamaki, H. Imahori, Y. Sakata, Y. Nishimura, I. Yamazaki, *Chem. Commun.* **1999**, 625.
[31] C. Luo, D. M. Guldi, H. Imahori, K. Tamaki, Y. Sakata, *J. Am. Chem. Soc.* **2000**, *122*, 6535–6551.
[32] D. M. Guldi, K.-D. Asmus, *J. Phys. Chem. A* **1997**, *101*, 1472.
[33] C. S. Foote, *Top. Curr. Chem.* **1994**, *169*, 347.
[34] H. Imahori, K. Tamaki, D. M. Guldi, C. Luo, M. Fujitsuka, O. Ito, Y. Sakata, S. Fukuzumi, *J. Am. Chem. Soc.* **2001**, *123*, 2607–2617.
[35] D. M. Guldi, M. Prato, *Acc. Chem. Res.* **2000**, *33*, 695.
[36] Agar (0.75 vol%) was added to an aqueous buffer solution (pH 7) and heated till the agar dissolved completely, the compound was dissolved in Triton X-100 and added to the solution at 60 °C, and a transparent jelly was formed after cooling to room temperature.
[37] a) U. Reuther, Ph.D. Thesis, University of Erlangen–Nürnberg (Germany), **2002**; b) L. Isaacs, A. Wehrsig, F. Diederich, *Helv. Chim. Acta* **1993**, *76*, 1231–1250.

Received: August 3, 2009
Published online: October 30, 2009

